

Inter- and Intramolecular C–H···O Bonding in the Anions of 1,3-Indandione Derivatives

Mark Sigalov,*^[a] Pnina Krief,^[a] Lev Shapiro,^{[a],‡} and Vladimir Khodorkovsky*^[b]

Keywords: Indandiones / Ionization / Hydrogen bonds

Derivatives of a series of 1,3-indandione (**1**) self-condensation products (**2–4**) and their anions (**2a–4a**) were investigated by NMR and UV/Vis spectroscopy and quantum mechanical calculations. These compounds exhibit a number of unusual features in their NMR spectra. Parent compound **1** is nearly not ionized in DMSO, whereas **3** is ionized completely. In contrast, derivatives **2** and **4** undergo partial ionization in DMSO and interaction between the neutral and anionic species affords the anionic intermolecular complexes, which exhibit both temperature- and concentration-dependent NMR spectra. The NMR spectra of pure salts **2a** and **3a**

are concentration independent, but temperature dependent. Charge delocalization in anions **2a** and **3a** gives rise to restricted rotation over the partial double bonds connecting the indane fragments. Energies of barriers to rotation were estimated from the temperature dependence of the ¹³C NMR spectra. The intramolecular aromatic C–H···O hydrogen bonding found previously in **2–4** is also observed in corresponding anions **2a–4a**.

(© Wiley-VCH Verlag GmbH & Co. KGaA, 69451 Weinheim, Germany, 2008)

Introduction

The diverse chemistry of 1,3-indandione [*1H*-indene-1,3(*2H*)-dione, **1**] attracts permanent interest, and this compound was first synthesized more than a century ago.^[1] As a valuable synthetic precursor, **1** or its derivatives have been employed in the synthesis of drugs (anticoagulants, analgesic, antiinflammatory medicines),^[2] in forensic chemistry for the detection of finger prints,^[3] as dyes, including NIR and pigments,^[4] and they have also been used as semi- and photoconductors.^[5] The 1,3-indandione-2-ylidene moiety exhibits strong electron accepting properties and its ability to accommodate a considerable negative charge was demonstrated by the synthesis of numerous “push–pull”-type chromophores with nonlinear optical properties.^[6] Derivatives of this type are usually prepared by the Knoevenagel condensation,^[7] which proceeds via the conjugate anions.

1,3-Indandione (**1**) is a moderately strong C–H acid with $pK_a = 7.2$.^[8] Orange enolate salts **1a** can be obtained by the addition of strong bases to its ethanol solutions.^[9] These salts are unstable, especially in solution, and in the presence of a neutral species, they rapidly form bindone [1,2'-biindene-1',3,3'(*2H*)-trione, **2**]. The high reactivity of anion **1a**

is also manifested by the fact that very pure samples of **1** can be stored in quartz vessels indefinitely long, but form **2** on prolonged contact with regular glass. Ease of self-condensation of **1** has already been mentioned in the paper describing its first preparation.^[1] A variety of the products were isolated depending on the reaction conditions, and the structure of a number of them had been misinterpreted. This quite complex reaction was recently reinvestigated and the correct structures of several products were unequivocally established by X-ray analysis (see ref.^[10] and the references cited therein).

Owing to the high reactivity of **1a**, its spectroscopic properties remain virtually unexplored. However, its surprisingly deep color attracted attention in connection with the antiaromaticity concept. The MINDO/3 optimized geometry of the anion showed an anomalous bond alternation in the five-membered ring,^[11] which was interpreted as a feature of antiaromaticity.

Of the self-condensation products of **1** that possess active methylene groups, derivative **2** was employed as an analytical reagent for amines and medicines involving the amino group.^[12] Although several reports cover such reactions of **2** like oxidation,^[13] alkylation,^[14] and condensation with aldehydes,^[15] this derivative and especially trindone (2'*H*-2,1':3',2''-terindene-1,1'',3,3''-tetrone, **3**) and their anions **2a** and **3a**, in spite of the astonishing ease of their formation, have never been subject of detailed studies. Owing to the strong electron-accepting properties and enhanced ability to delocalize a negative charge, they deserve more attention, in particular, as potential precursors of NLO chromophores. Indeed, the anions of **2** and **3** are deeply colored

[a] Department of Chemistry, Ben-Gurion University of the Negev, 84105 Beer-Sheva, Israel
Fax: +972-8-6472943
E-mail: msigalov@bgu.ac.il

[b] Université de la Méditerranée, UMR CNRS 6114, 13288, Marseille 09, France
E-mail: khodor@luminy.univ-mrs.fr

‡ Deceased.

Supporting information for this article is available on the WWW under <http://www.eurjoc.org> or from the author.

and the product of condensation of **2** with *p*-diethylaminocinnamic aldehyde exhibited unusual photochromic properties and high hyperpolarizability in its “open” form.^[16]

As typical 1,3-diketones, derivatives **1–3** could potentially form enols. However, except in the case of **1** bearing sterically demanding 2-diarylmethyl substituents,^[17] the enol forms were never observed.

Recently, we demonstrated^[18] that the molecular geometry of derivatives **2–4** allows formation of intramolecular hydrogen bonds between the aromatic C–H atoms and oxygen atom of one of the carbonyl groups. At the same time, when the ¹H and ¹³C NMR spectra of these derivatives were studied in polar solvents, we observed a number of irregularities (e.g., signal broadening), which can stem from partial ionization of the neutral species. The spectra of anionic species **1a–4a** have never been studied. Here we report the spectroscopic (NMR and UV/Vis) and quantum mechanical investigation of the anions derived from **1** and the products of its self-condensation (**2–4**).^[10] We show that the broadening of the NMR signals of neutral **2** and **4** in

DMSO is a result of intermolecular hydrogen-bonded anionic complex formation. The broadening of the NMR signals of pure anions **2a** and **3a** at low temperatures results from restricted rotation over partial double bonds linking the indane moieties, and intramolecular hydrogen bonding in the anions is even stronger than that observed for the neutral species.

Results and Discussion

Preparation of the Anions

Bindone and trindone anions **2a** and **3a** are stable and can be isolated as tetrabutylammonium salts by the addition of tetrabutylammonium hydroxide to THF solutions of **2** and **3**. The salt of **1** is unstable and anion **1a** was generated in solution by adding 1,8-diazabicyclo[5.4.0]undec-7-ene (DBU). Addition of a slight excess of DBU to solutions of the neutral compounds resulted in complete ionization of all studied derivatives. The NMR and UV/Vis spectra of anions **2a** and **3a** obtained preparatively and generated in solution by the addition of DBU were identical. Each anion exhibits an intense long wavelength absorption band in the visible range (two bands in the case of **4a**, Figure 1) involving more or less pronounced vibronic splitting. The increase in the number of the indanone moieties leads to considerable bathochromic shifts of the longest wavelength band. Solutions of **2a** are red-violet, whereas those of **3a** are green and those of **4a** are blue. The TD DFT method reproduces these experimental results reasonably well. Thus, the TD B3LYP method coupled with the 6-31+G(d,p) basis set predicted the first electronic transitions as HOMO→LUMO transitions: 426, 495, 639 and 636 nm for **1a–4a**, respec-

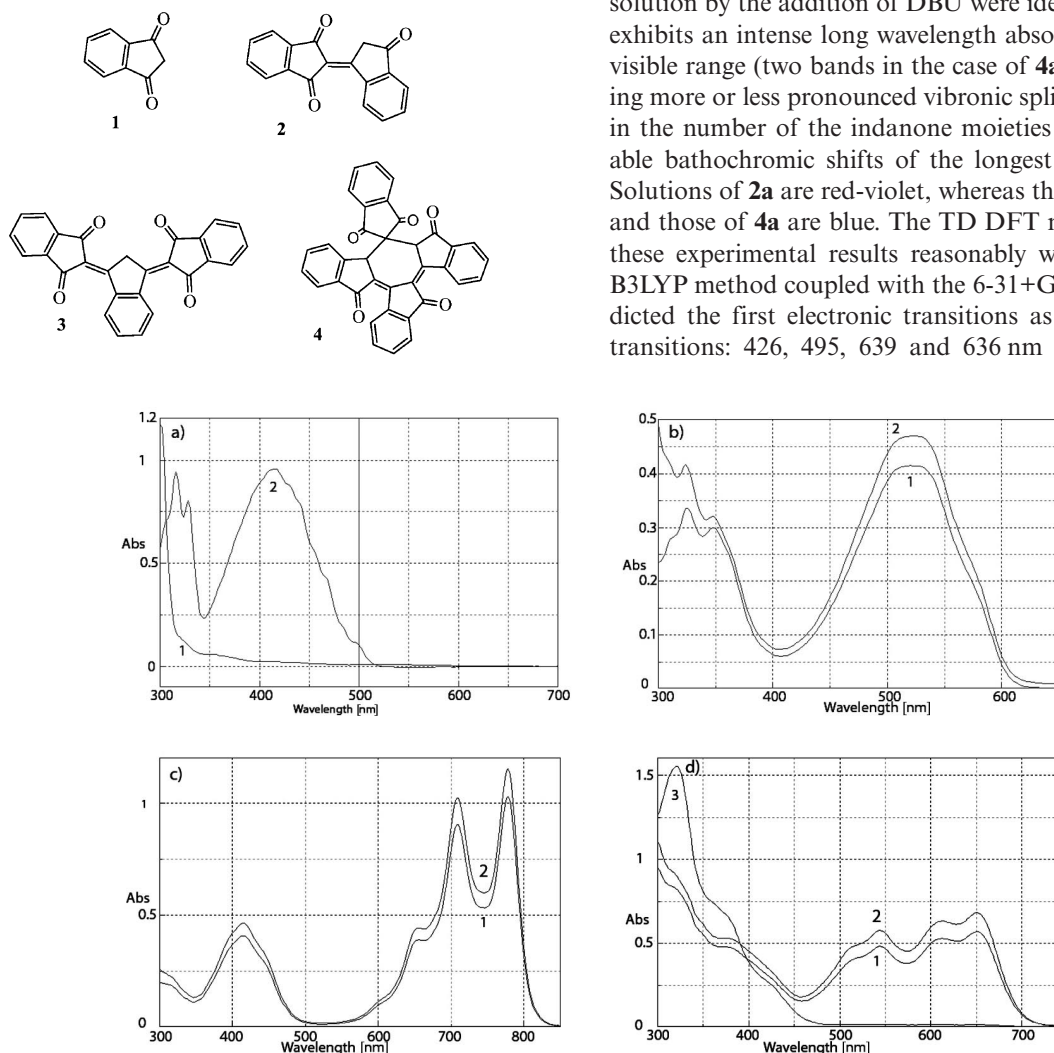
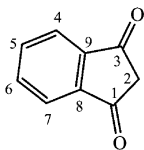
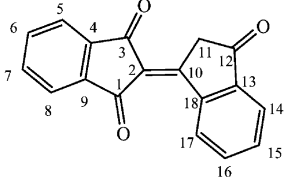
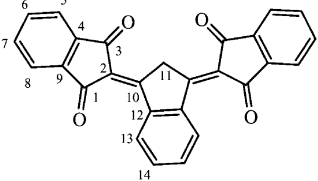


Figure 1. UV/Vis spectra of (a) **1a**, (b) **2a**, (c) **3a**, (d) **4a** in DMSO. 1 – solutions of the neutral species, 2 – after addition of DBU, 3 – addition of CF₃COOH.

Table 1. Selected experimental (CD₂Cl₂) and calculated [B3LYP/6-31G(2d,2p)] ¹H and ¹³C NMR chemical shifts for derivatives **1–3** and **1a–3a**.^[a]

								
1, 1a			2, 2a			3, 3a		
	1	$\delta_{\text{exp.}}$ [ppm] 1a	$\Delta\delta^{[b]}$		1	$\delta_{\text{calcd.}}$ [ppm] 1a	$\Delta\delta^{[b]}$	
2-H	3.25	4.50	1.25		2.60	3.95	1.35	
C-1,3	198.1	193.1	–5.0		191.7	182.4	–9.3	
C-2	43.5	94.3 (164.1) ^[c]	50.8		45.4	93.5	48.1	
	2	$\delta_{\text{exp.}}$ [ppm] 2a	$\Delta\delta$		2	$\delta_{\text{calcd.}}$ [ppm] ^[d] 2a	$\Delta\delta$	
11-H	4.18	6.67	2.49		3.73	6.82	3.09	
17-H	9.69	8.73	–0.96		9.48	8.74	–0.74	
C-1	189.3	191.5	2.2		185.1	184.2	0.9	
C-2	125.8	105.3	–20.5		126.4	107.5	–18.9	
C-3	190.6	191.5	0.9		186.3	184.2	–2.1	
C-10	156.3	159.2	2.9		158.9	157.3	–1.6	
C-11	43.4	110.4 (172.7) ^[c]	67.0		46.7	111.6	64.9	
C-17	131.6	126.9	–4.7		132.1	126.3	–4.8	
	3	$\delta_{\text{exp.}}$ [ppm] 3a	$\Delta\delta$		3	$\delta_{\text{calcd.}}$ [ppm] 3a	$\Delta\delta$	
11-H	5.15	8.68	3.53		4.97	9.87	4.90	
13-H	9.83	8.98	–0.85		10.65	10.22	–0.43	
C-2	124.9	112.0	–12.9		126.8	118.2	–8.6	
C-10	161.2	158.5	–2.7		163.3	161.7	–1.6	
C-11	42.4	115.7 (177.5) ^[c]	73.3		47.6	120.6	73.0	

[a] Full data are given in the Supporting Information (Table S1). [b] The difference in the chemical shifts of the corresponding nuclei in the anion and neutral compound. [c] The one-bond constants $^1J(^{13}\text{C}, ^1\text{H})$ for selected carbon atoms are given in parentheses. [d] Calculation for partially optimized geometry of **2** and **2a** (see the text).

tively. A second low-energy transition at 585 nm [HOMO→LUMO (+1)] was calculated for **4a**, which is in agreement with the experiment. Geometry optimizations were done at the same level. It is noteworthy that the use of diffuse orbitals is not crucial for these delocalized anions, as the geometries optimized by using the 6-31G(d,p) basis set were almost identical. Moreover, the excited-state energies calculated with and without the use of diffuse orbitals differed only by a few nanometers. For example, for **1a**, the calculations yielded 426 nm [B3LYP/6-31+G(d,p)//B3LYP/6-31+G(d,p)], 423 nm [B3LYP/6-31G(d,p)//B3LYP/6-31+G(d,p)], and 418 nm [B3LYP/6-31G(d,p)//B3LYP/6-31G(d,p)].

The ¹H NMR spectra show, besides significant changes in the chemical shifts of the aromatic protons, the disappearance of the signals corresponding to the active methylene group protons and, in the case of **1–3**, the appearance of new signals corresponding to the protons at the sp²-hybridized carbon atoms is observed (see Table 1).

Ionization in DMSO and Intermolecular C–H···O[–] Bonding

The relative acidities of **1–4** can roughly be estimated by the degree of their ionization in DMSO. Thus, the dissol-

ution of derivative **1** in DMSO is accompanied by a very weak pink coloration, whereas **2** gives a more intense red-violet color, **3** an intense green color, and **4** a deep blue color, which indicates a considerable degree of ionization for derivatives **2–4**. Indeed, whereas the UV/Vis spectrum of **1** does not show the presence of a noticeable amount of **1a**, the spectra of derivatives **2** and **3** almost do not change upon the addition of DBU (Figure 1). Addition of an excess amount of CF₃COOH brings about almost complete protonation of **4a**, but anion **2a** only underwent full protonation after the addition of a very large excess of the acid. Anion **3a** cannot be protonated even by a large excess of CF₃COOH.

In agreement with this, only the signals of **1** are present in the ¹H NMR spectrum in [D₆]DMSO solution. The solution of **3** does not show signals of the neutral compound but only those of the anion. These signals are slightly broadened, but the addition of a small quantity of DBU leads to their narrowing. At the usual NMR concentrations (ca. 5 × 10^{–2} M), compound **2** is only partially ionized – signals for the two species are present (Figure 2). One of them (major) is the neutral nonionized bindone, but the second one (minor) shows signals whose chemical shifts and line-

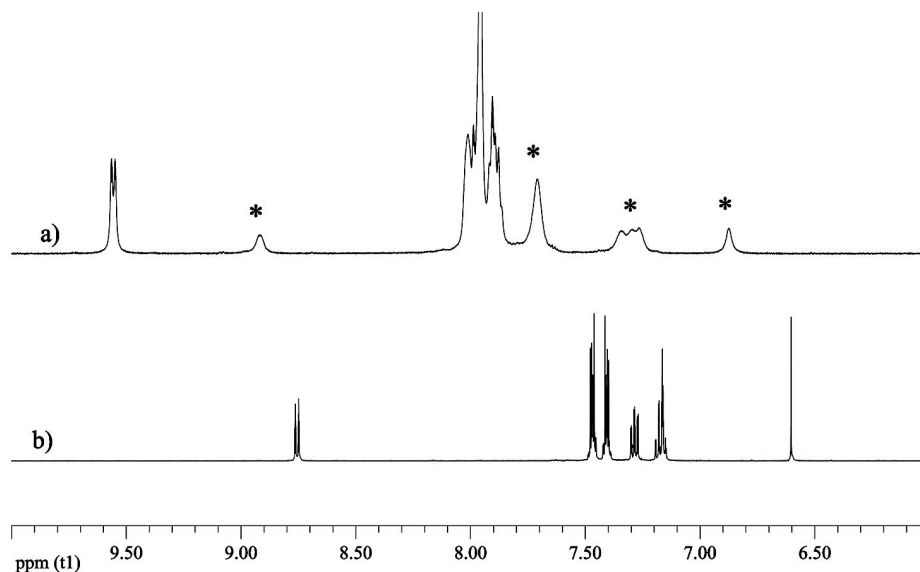


Figure 2. The aromatic parts of the spectra of bindone **2** (a) and its salt **2a** (b) in $[D_6]DMSO$. The signals of the minor component (dimeric anionic complex) are marked by the asterisks.

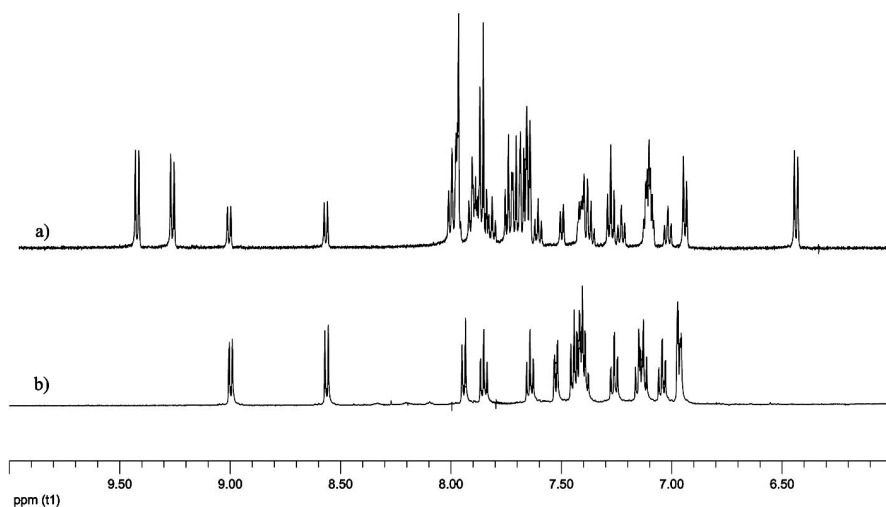
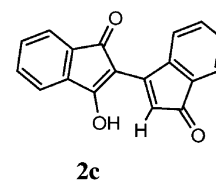
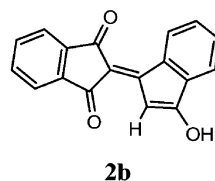


Figure 3. The aromatic parts of the spectra of tetramer **4** (a) and **4a** in the presence of DBU (b) in $[D_6]DMSO$.

shapes significantly differ from the corresponding signals of pure bindone anion **2a** in $[D_6]DMSO$. Consecutive dilutions of a solution of **2** in $[D_6]DMSO$ (Supporting Information, Figure S1) increased the relative intensity of the signals of the initially minor component of the mixture; the signals move towards the positions corresponding to the anion. Partial ionization is also observed upon dissolution of **4** in $[D_6]DMSO$. However, unlike the case of **2**, the spectrum of the minor component is more similar to the spectrum of the anion with regard to the chemical shifts and the signal widths (Figure 3).

The enol tautomeric forms of compounds **1–4** cannot be detected. The 1H and ^{13}C NMR spectra of anions **2a**, **3a**, and **4a** in $[D_6]DMSO$ are almost identical to the spectra of these compounds in CD_2Cl_2 in the presence of DBU (except

for the obvious minor solvent effect on the chemical shifts). Quantum mechanical calculations [B3LYP/6-31G+(d,p), ZP corrected] show that both possible enol forms **2b** and **2c** are less stable than the triketo form **2** by 10.7 and 20.3 kcal mol $^{-1}$, respectively. Thus, the existence of the free enol forms can safely be excluded from consideration.



Anionic Complex Formation

The ^1H NMR spectra of both **2** and **4** in $[\text{D}_6]\text{DMSO}$ are temperature dependent but in different manner. The signals of both neutral and anionic species of **2** are broadened at 298 K. The increase in temperature brings about further signal broadening and at 340 K, the signals of the second component disappear (Supporting Information, Figure S2). In the spectrum of tetramer **4**, all signals are well resolved in the temperature range between 298 and 330 K. The signals are broadened at temperatures higher than 330 K, but the complete coalescence of the signals does not occur even at 390 K (Supporting Information, Figure S3).

These temperature changes are reversible regarding the width of the signals. The relative intensities of the both species after cooling to room temperature remain the same for **2**. Derivative **4** slowly decomposes in DMSO at high temperatures. The narrow temperature range of signal broadening for **2** and a wider one for **4** indicate the relatively fast proton exchange in the first case and relatively slow in the second.

Reversible broadening and a tendency toward coalescence of those signals that stem from the anionic and neutral species are features of their interconversion. The observed phenomenon can be explained by proton migration from the acidic methylene group of the neutral form to the sp^2 carbon of the anion. Such exchange is possible within complexes **2a**···**2**, **3a**···**3**, and **4a**···**4** bound by the ionic hydrogen bonds, as observed for 2-phenyl-1,3-indandione and dime-done.^[19] From the above-mentioned ^1H NMR spectral behavior of the DMSO solutions (the significant difference between the spectra of anion **2a** and the minor component of **2** on the one hand, and close similarity of the spectra in the case of **4**, together with the different temperature dependence for **2** and **4**) it follows that this complex should be stronger and its concentration much higher for **2** than for **4**. Close similarity observed for the spectra of both **3** and **3a** in $[\text{D}_6]\text{DMSO}$ may be explained not by the weakness of the complex but by the absence of the neutral component (necessary for complex formation) due to almost complete ionization.

Quantum mechanical calculations show that formation of a complex between **2** and **2a** stabilized by two C–H···O hydrogen bonds is indeed possible. Geometry optimizations starting from different initial configurations gave several local minima with the energy gain of 1–2 kcal mol^{−1}. However, most of the initial structures yielded a complex shown in Figure 4. The energy gain for this complex formation was 16.6 kcal mol^{−1}.

Proton exchange within such complex proceeds through the intermediate unstable enol form **2b**.

The direct experimental evidence of the proton exchange was obtained from the 2D NOESY experiment (Figure 5). Here, the 1D projections correspond to the ^1H NMR spectrum shown in Figure 2. All cross peaks observed in the spectrum (particularly, between the signals at $\delta = 9.4$ and 8.9 ppm, between the signals at 4.1 and 6.5 ppm, and between the signals at 7.1 and 8.0 ppm) indicate the exchange

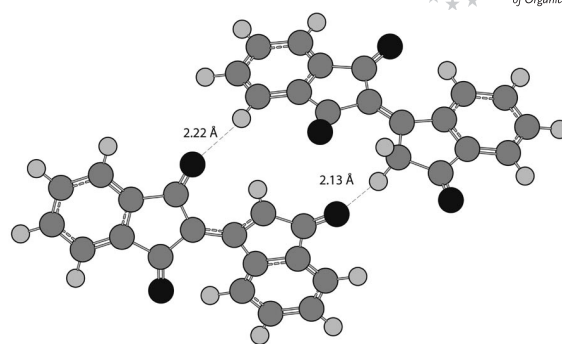
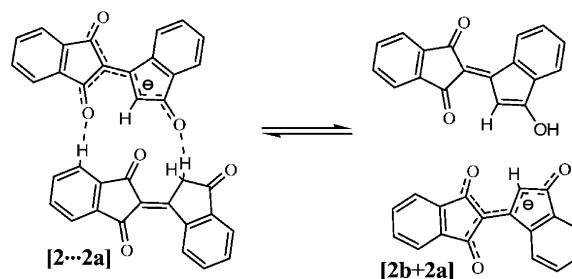


Figure 4. The geometry of the **[2...2a]** complex [B3LYP/6-31G(d,p) optimization].



process between similar protons in different moieties. This result unambiguously confirms the existence of proton exchange between the **2** and **2a** species.

In order to exclude the possibility that proton exchange occurs through the solvent molecules, the rate constants of this transfer at different concentrations were calculated by the NMR line-shape analysis. The experimental and calculated spectra of a concentrated bindone solution in $[\text{D}_6]\text{DMSO}$ before and after a 10-fold dilution are shown in Figure 6. The average number of solvent molecules separating the solute species should increase by $10^{1/3}$, that is, more than twice upon 10-fold dilution, and the rate constants should decrease correspondingly in the case of the solvent mediated exchange. As shown in Figure 6, the rates of the proton exchange remain roughly the same at both concentrations, which unambiguously proves the intramolecular proton transfer that may take place only within a complex such as **2**···**2a**. Analogous treatment of the experimental spectra was also carried out for the $[\text{D}_6]\text{DMSO}$ solution of **4** (Supporting Information, Figure S4).

Substitution of the rate constant values into the Eyring equation afforded the following free activation energies ΔG^\ddagger_{350} for the observed dynamic processes: 16.9 kcal mol^{−1} for **2**···**2a** and 18.7 kcal mol^{−1} for **4**···**4a**. This is in good agreement with the above assumption of the lower stability of the latter complex.

The same complexes should also form in less-polar solvents like chloroform when the anionic form, which in this case cannot appear as a result of ionization, is added. Indeed, it is observed in the ^1H NMR spectra of mixtures of **2** and **2a** in CDCl_3 solution. Each component of the mixture gives sharp signals at 260–315 K, but at 320 K and

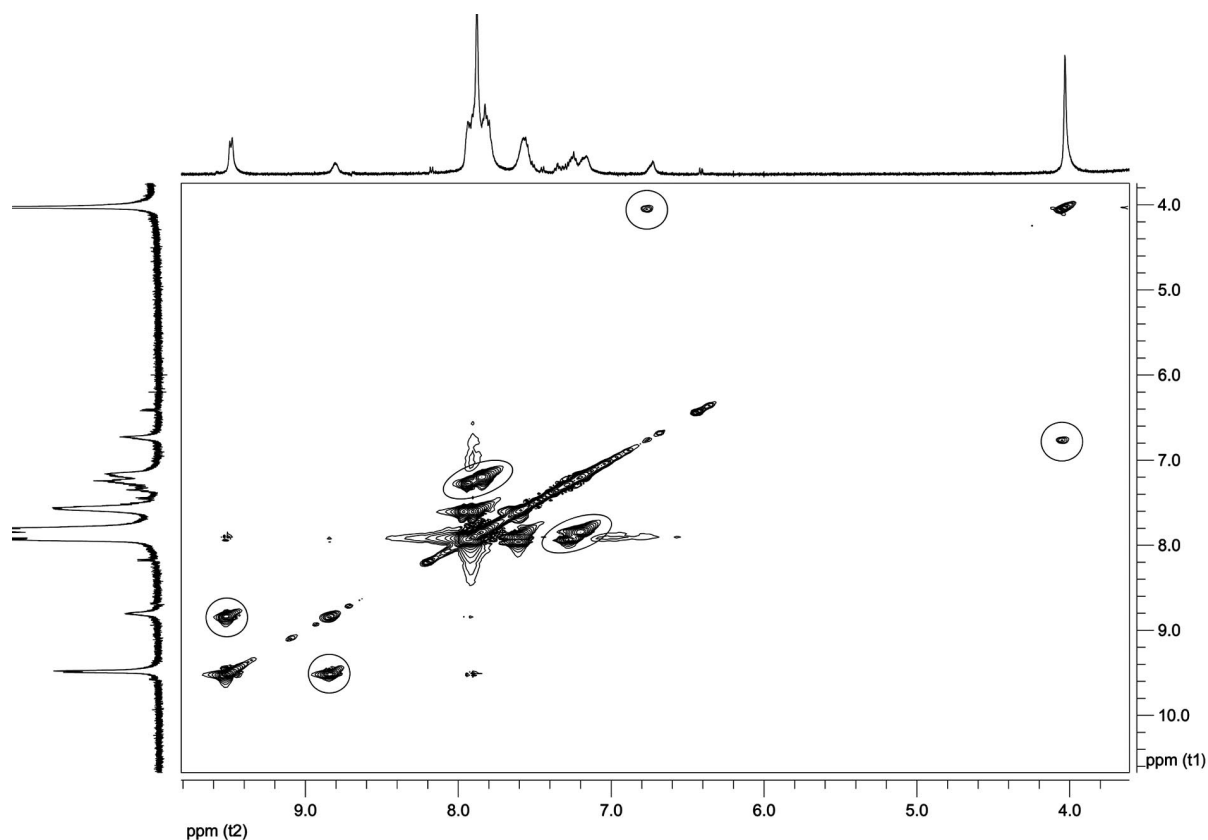


Figure 5. 2D NOESY spectrum of bindone **2** in $[D_6]$ DMSO at room temperature. The highlighted cross-peaks indicate the exchange relationship between similar protons of the different moieties.

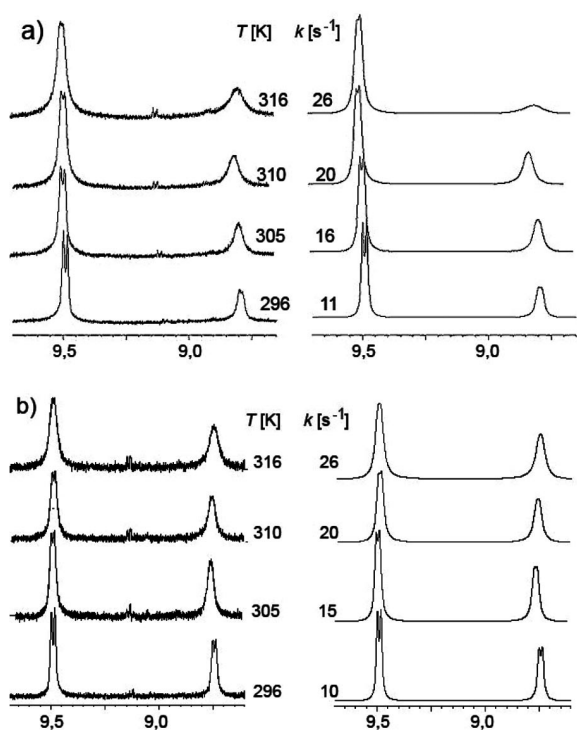


Figure 6. Observed (left) and calculated (right) variable-temperature 1H NMR spectra of bindone **2** in $[D_6]$ DMSO: (a) saturated solution (neutral bindone/complex, 2:1), (b) 10-fold dilution (neutral bindone/complex, 1.3: 1).

above, the signals are broadened. However, proton exchange between both species is observed at 305 K and is proved by 2D NOESY spectroscopy; the spectrum is quite similar to the above-mentioned 2D NOESY spectrum in $[D_6]$ DMSO (Supporting Information, Figure S5).

In light of these considerations, it is possible to explain the behavior of **2** in DMSO solution as follows. There is equilibrium between the three species in solution: neutral **2**, its anion **2a**, and dimeric complex **2...2a**. The proton exchange between the dimeric complex and the excess amount of the free anion is fast on the NMR timescale and gives rise to the appearance of the averaged broad signals (marked by the asterisks in Figure 2). The proton exchange between neutral molecules **2** and anionic complex **2...2a** is sufficiently slow on the NMR timescale to afford the separate signals, but participation of both neutral species and the anionic complex in exchange is proved by the NOESY experiment. Both exchange processes are accelerated at higher temperatures, and further broadening and eventual coalescence of all signals is observed (Supporting Information, Figure S2). Dilution of the solution brings about further ionization of the neutral molecules. Anions **2a**, which form upon dilution, bind further quantities of the neutral molecules to form dimeric complex **2...2a**. As a result, the concentration of **2** diminishes, and the average signals of **2a** and **2...2a** increase and move towards their positions observed in the spectrum of the pure anion (Supporting Information, Figure S1).

Thus, the temperature and concentration dependence of the NMR spectra of derivatives **2–4** in polar solvents stem from their partial ionization and strong interaction of the resulting anions with the neutral species.

Delocalization of the Negative Charge and Geometry of the Anionic and Neutral Species

The representative bond lengths corresponding to the optimized equilibrium geometries [HF/6-31G(d,p)] of compounds **1–4** and their anions **1a–4a**, together with the sum of the Mulliken charges on each indane moiety, are given in Scheme 1. Expectedly, ionization brings about considerable changes in the structures of the studied compounds.

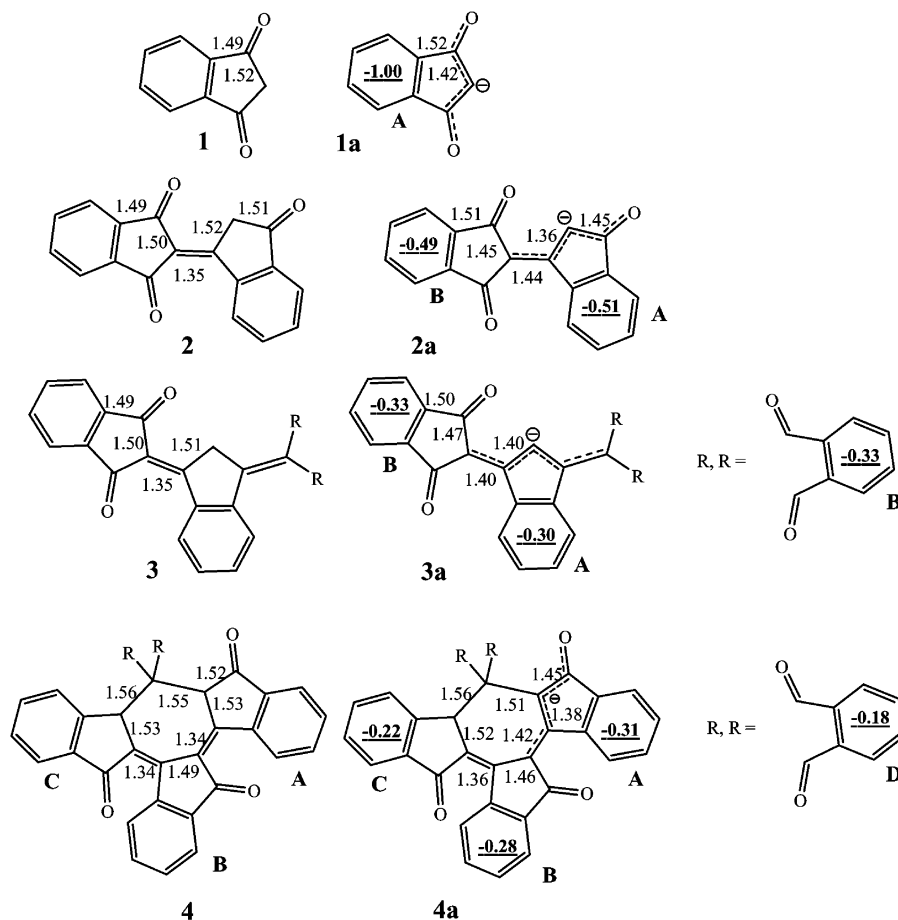
As expected, ionization results in shorter C–C bonds between the carbonyl groups in the five-membered rings of the indane moieties and longer bonds connecting these moieties. The changes are smaller with increasing delocalization of the negative charge (one per one indane unit in **1a**, one per two indane units in **2a**, and one per three indane units in **3a** and **4a**). Noteworthy, the charge is evenly distributed over the indane moieties of **2a** and **3a**, whereas it consequently diminishes in the A-, B- and C-indane moieties of **4a**. Somewhat surprising is the significant negative charge on the nonconjugated D moiety of **4a**. In fact, this charge

mostly stems from the increase in the negative charge (by -0.08) on the spirocyclic atom, and the bond connecting the A and D moieties is shortened by 0.04 Å.

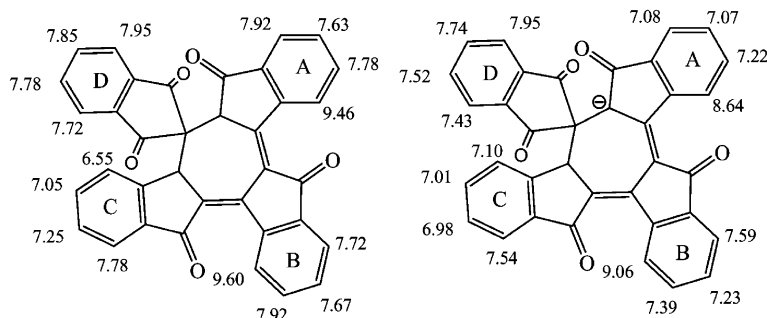
Thus, the degree of charge delocalization increases in the order **1a** < **2a** < **4a** < **3a**, and in the same order the bathochromic shift of the longest wavelength absorption bands in the UV/Vis spectra increases. The corresponding calculated [B3LYP/6-31G+(d,p)] energy gaps between the HOMO and LUMO (eV) decreases in this order as well: 0.130 for **1a**, 0.111 for **2a**, 0.095 for **4a**, and 0.085 for **3a**.

The NMR Spectra of Anions **1a–4a**

Comparison of the ^1H and ^{13}C NMR chemical shifts in the anions and the neutral precursors provides a reasonable experimental estimation of the degree of charge delocalization. The experimental ^1H NMR chemical shifts of the aromatic hydrogen atoms of **4** and **4a** are shown in Scheme 2. In general, the calculated shifts are in good agreement with the experimental ones and enable assignment of all the signals. Comparison of the chemical shift changes stemming from ionization (the difference in chemical shifts of the corresponding nuclei in the anion and the neutral compound, denoted as $\Delta\delta$ in Table 1) reveals the following features. The



Scheme 1. Optimized [HF/6-31G(d,p)] bond lengths (Å) in **1–4** and **1a–4a** and the total charges [B3LYP/6-31G(d,p)] on the indane moieties of **1a–4a** (in bold underlined). Capital letters A, B, C, D denote the molecular fragments.



Scheme 2. The experimental ^1H NMR chemical shifts in **4** and **4a**.

most dramatic changes in the chemical shifts (Table 1) are observed for those carbon atoms for which their C–H bonds underwent ionization (C-2 for **1**, C-11 for **2**, and **3**), and the changes are mainly due to the change in hybridization from sp^3 to sp^2 . Both the δ values ($\delta = 94.3$, 110.4 , and 115.7 ppm, respectively) and $\Delta\delta$ values ($\delta = 50.8$, 67.0 , and 73.3 ppm, respectively) indicate increase in charge delocalization on going from **1a** to **3a**, that is, the larger the number of the indane units, the smaller the negative charge on the ionized carbon atom.

The carbon atoms of the double bond connecting the indane fragments in **2** and **3** (especially C-2) are also very sensitive to ionization. The $\Delta\delta$ of C-2 are -20.5 ppm for **2a** and -12.9 ppm for **3a**, which indicates the presence of a significant negative charge on this atom. The difference in the chemical shifts of C-2 and C-10, both for the neutral molecules and for the anions, provides some information about the relative polarity of the connecting double bonds and the partial double bonds. These differences are: 30.5 and 53.9 ppm for **2** and **2a**, respectively, and 36.3 and 46.5 ppm for **3** and **3a**, respectively. That is, the polarities (and the bond orders) of the connecting bonds are much more different for **2** and **2a** than for **3** and **3a**. It is in good agreement with the results of dynamic NMR (see below) and with the optimized geometry of these species (in particular, the lengths of the connecting bonds that are the same – 1.35 Å both for **2** and **3**, but different for **2a** – 1.44 Å and for **3a** – 1.40 Å).

Of the carbonyl carbon atoms, the most sensitive to the anion formation are only those situated in direct proximity to the ionized carbon atom. These are C-1,3 in **1a** ($\Delta\delta = -5.0$ ppm) and C-12 in **2a** ($\Delta\delta = -4.0$ ppm). The remote carbonyl carbon atoms are much less sensitive.

Intramolecular Aromatic C–H \cdots O Bonding in **2a–4a**

Recently, we demonstrated^[18] that the geometry of the C–H \cdots O=C fragments of derivatives **2–4** meet the criteria, which set the limits for possible C–H \cdots O hydrogen bonding occurrence.^[20] A detailed NMR spectroscopic and quantum mechanical study revealed the following manifestations of hydrogen bonding: (1) large low-field chemical shifts of the protons and carbon atoms involved, (2) increase in the one-bond ($^{13}\text{C}, ^1\text{H}$) spin–spin coupling constants, and (3) non-

zero positive values of the overlap coefficients between the orbitals involving the interacting oxygen and hydrogen atoms. The methodology developed in ref.^[18] was applied to anions **2a–4a**.

All features of hydrogen bonding found recently in neutral molecules **2–4** are also present in the NMR spectra of the anions (Table 1 and Scheme 2). Thus, for **2a**, the ^1H NMR chemical shift difference between the bonded hydrogen (17-H) and its counterpart in the *para* position (14-H) is 1.50 ppm. The ^{13}C NMR chemical shift difference between the corresponding carbon atoms (C-17 and C-14) is 8.2 ppm. The one-bond coupling constant $^{13}\text{C}–^1\text{H}$ for C-17 is 166 Hz, whereas that for C-14 is 163 Hz.

Hydrogen atoms in the CH_2 groups of neutral **2** and **3** cannot be involved in hydrogen bonds for the geometric reasons we showed earlier.^[18] However, the hydrogens at the sp^2 carbon atoms in anions **2a** and **3a** meet the above-mentioned criteria^[20] and are hydrogen bonded. This is supported by an increase in the respective one-bond coupling constants $^1J(^{13}\text{C}, ^1\text{H})$ from 164.1 Hz for C-2 in **1a** to 172.7 Hz for C-11 in **2a**, and to 177.5 Hz for C-11 in **3a** (Table 1).

The optimized geometries of **2** and **2a** exhibit an interesting feature: the through-space O \cdots H distance in **2a** becomes slightly shorter (2.06 and 2.03 Å, respectively) in spite of the noticeable (0.09 Å) increase in the central C–C bond length (Scheme 1). The same trend is observed for **3** and **3a**: the O \cdots H distance in both molecules is 2.03 Å, whereas the central bond is longer for **3a** by 0.05 Å. Similarly, the C–H \cdots O distances in both hydrogen-bonded fragments of **4a** are shorter than their analogs in **4** (2.06 and 2.15 Å, respectively, for fragment A and 2.02 and 2.14 Å, respectively, for fragment B) in spite of sufficient increase in connecting bonds lengths upon ionization (Scheme 1).

Therefore, the hydrogen bond in the anions should be stronger. The reason of this may be a substantial increase in the negative charge on the oxygen atom. Both *ab initio* and DFT geometry optimizations provide generally good agreement with the experimental values, although the hydrogen bonding strength is overestimated. Thus, for bindone **2** the optimized O \cdots H distances (2.02 – 2.07 Å depending on the calculation method^[18]) were shorter than the experimental value of 2.18 Å;^[21] consequently, the calculated [B3LYP/6-31G(2d,2p)] chemical shifts of the

bonded hydrogen atom were by 0.8–1.2 ppm larger than the experimental value of 9.69 ppm as a result of the more pronounced influence of the carbonyl carbon atom. The other calculated chemical shifts were in excellent agreement with the experimental values (deviations within 0.1–0.2 ppm for ^1H and 2–3 ppm for ^{13}C). Optimization of the geometry of **2** with a fixed O···H distance of 2.20 Å reproduced the experimental nonplanarity of the molecule^[18,21] and subsequent calculation of the NMR chemical shifts gave much better agreement with the experimental values ($\delta = 9.48$ ppm instead 10.38 ppm in comparison to the experimental value of 9.69 ppm, Table 1). It was concluded that the partially optimized geometry of bindone is very close to the real geometry in solution.^[18]

A similar partial optimization with a fixed O···H distance of 2.20 Å was carried out for **2a**. The calculated chemical shifts for the partially optimized anion **2a**, especially those for the atoms in the vicinity of the hydrogen-bonded fragment, agree with the experimental values fairly well (8.74 vs. 8.73 ppm for 17-H, and 126.9 vs. 126.3 ppm for C-17, Table 1).

C–H···O Hydrogen Bond in Model Complexes

Demonstration of stronger hydrogen bonding involving anions relative to that involving neutral species raises the problem of evaluation, even approximate, of its energies in both cases. The influence of the negatively charged oxygen atom on the hydrogen bonding strength can be estimated by comparing two analogous hydrogen-bonded complexes of **1** and **1a** with benzene. The energy minima [at the B3LYP/6-31G+(d,p) level] correspond to the O···H distance of 2.62 Å in the [**1**···C₆H₆] complex and of 2.17 Å in the [**1a**···C₆H₆] complex. Both complexes are stabilized by 1.0 and 4.0 kcal mol^{−1}, respectively, relative to the noninteracting components. It should be emphasized that these val-

ues present lower limits of the hydrogen-bond energies, as the benzene molecule is a relatively weak hydrogen donor.

Dynamic NMR and Restricted Rotation in Anions **2a** and **3a**

As we have demonstrated above, the calculation results and the NMR chemical shifts indicate that charge delocalization in the anions increases in the order **1a** < **2a** < **4a** < **3a**. Such delocalization increases the bond order of the bonds connecting the indane moieties and may result in the appearance of rotational barriers in anions **2a** and **3a**. The ^1H NMR spectra of **2** and **2a** in CD₂Cl₂ are shown in Figure 7. The two aromatic rings of bindone give two four-proton spin systems, one of them is a first-order spectrum and consists of two doublets and two triplets and the other one (corresponding to the 2-substituted 1,3-indandione moiety) is a system that can be assigned to the ABCD-type (Figure 7a). Formation of the anion, along with the high-field shift of all aromatic protons owing to the negative charge, also brings about transformation of the asymmetrical ABCD system into the symmetrical AA'BB' one (Figure 7b). This part of the spectrum is temperature dependent and broadening and decoalescence of the signals occurs below 200 K (Figure 7c).

The ^{13}C NMR spectrum of **2a** at room temperature shows similar features. The 1,3-indandione moiety shows only five carbon signals instead of nine (Table 1). Some of these signals decoalesce with decreasing temperature and at 180 K the spectrum involves separate signals corresponding to each carbon atom of the 1,3-indandione fragment. These spectral changes indicate the presence of restricted rotation over the partial double bond connecting the indane fragments. The spectra of **3a** exhibit the similar behavior. In both cases, however, the slow exchange limit in the ^1H NMR spectra was not reached and the rotation process

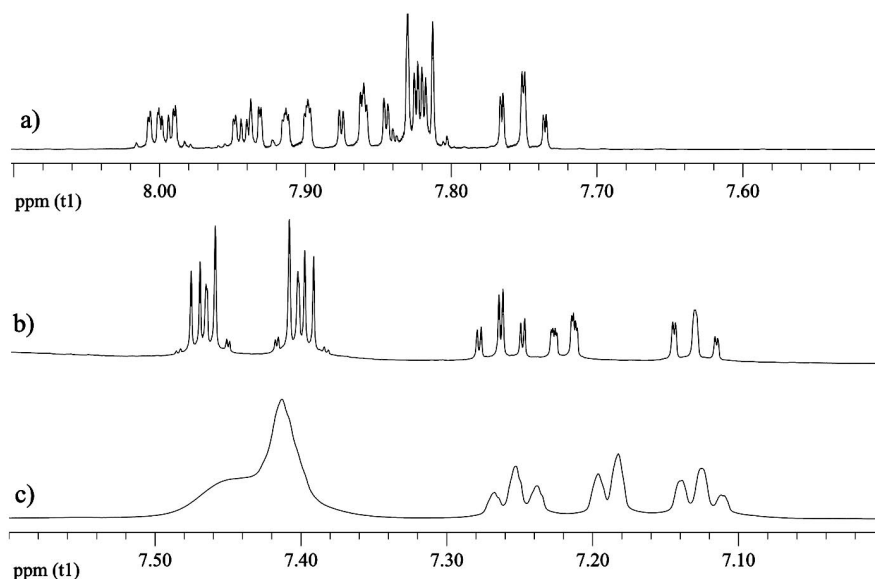


Figure 7. The temperature dependent part of the ^1H NMR spectra of **2** (a) and **2a** at room temperature (b), and at 180 K (c).

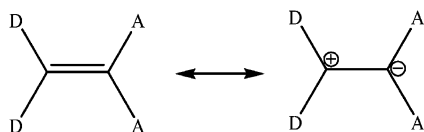
monitoring was carried out by using ^{13}C NMR (Supporting Information, Figure S5).

The barriers to rotation were estimated from the temperature dependences of the ^{13}C NMR spectra of **2a** and **3a**. Two pairs of peaks undergoing coalescence in the spectra of both substances were found to be the most suitable for the dynamic NMR analysis and the rotational barriers were calculated as the average values of free energy of activation at the coalescence temperatures (Table 2).

Table 2. Kinetic parameters of rotation over the $\text{C}_2\text{--C}_{10}$ bonds in **2a** and **3a**.

Entry	Probe	$\Delta\nu$ [Hz]	T_c [K]	k [sec^{-1}]	ΔG^\ddagger [kcal mol^{-1}]
2a	C-5, C-8	63	200	140	9.6
	C-4, C-9	27	195	60	9.7
3a	C-5, C-8	55	235	122	11.3
	C-4, C-9	14	220	31	11.4

The barrier to rotation in **2a** is about $1.7 \text{ kcal mol}^{-1}$ lower than the barrier measured for **3a**, which is in agreement with the results of quantum mechanical calculations that show considerably shorter and stronger connecting bonds in **3a** relative to those in **2a**. The ^{13}C NMR chemical shifts give the additional experimental evidence of relative strength of these bonds. It is known^[23] that rotational barriers over partial double bonds in push–pull ethylenes decrease with increasing bond polarization.



Increasing polarization, in turn, is reflected by enhancing the difference between the ^{13}C NMR chemical shifts of the involved carbon atoms. In our case, the anionic center serves as the electron-donor moiety and the 1,3-indandione fragment is the acceptor. The chemical shift difference between C-2 and C-10 is 53.9 ppm in the bindone anion and 42.8 ppm in the trindone analog. That is, the bindone anion contains a more polarized connecting bond with a relatively smaller bond order resulting in a lower barrier to rotation.

Conclusions

The NMR spectra of derivatives **2** and **4** in $[\text{D}_6]\text{DMSO}$ are temperature and concentration dependent as a result of their partial ionization. The neutral and anionic species form intermolecular hydrogen bonded anionic complexes, which thus enables exchange of the acidic hydrogen atom. In turn, the NMR spectra of pure anions **2a** and **3a** are concentration independent, but temperature dependent owing to restricted rotation about the partial double bonds connecting the indane moieties. These bonds in **3a** are closer to double bonds owing to the higher degree of negative charge delocalization, and the barrier to rotation in this derivative is therefore, by $1.7 \text{ kcal mol}^{-1}$, higher than that of

2a. The intramolecular anionic hydrogen bonds observed in anions **2a–4a** are stronger than those observed in neutral derivatives **2–4**.

Experimental Section

General: ^1H and ^{13}C NMR spectra were recorded at 500 and 125 MHz, respectively, in CDCl_3 (CD_2Cl_2 for low-temperature measurements) and $[\text{D}_6]\text{DMSO}$ solutions. The temperature unit was calibrated by using the samples of methanol and ethylene glycol with the accuracy of $\pm 1^\circ$. The assignment of the ^{13}C signals of the $\text{C–H}\cdots\text{O}$ fragments was performed by the 2D HXCORR technique. 2D NOESY spectra were run by using standard Bruker software (noesyph pulse program).

Quantum-mechanical calculations were performed by using Gaussian 03W software.^[24] The geometry optimization for compounds **1–4** and their anions **1a–4a** was carried out with the HF/6-31G(d,p) model chemistry^[25] as a reasonable compromise between cost and accuracy, especially for large molecules **3** (**3a**) and **4** (**4a**). The geometry of anionic complex **2 \cdots 2a** and its components was optimized by using the DFT method^[26] (B3LYP) with the use of the 6-31G(d,p) basis set. Single-point calculations were also done by using the B3LYP method: the energies of anions **1a–4a** as well as energies of hypothetical enol forms of bindone (**2b** and **2c**) were calculated with the 6-31G+(d,p) basis set, and the ^1H and ^{13}C NMR chemical shifts were calculated by the GIAO method^[27] with the use of the 6-31G(2d,2p) basis set, as it gives the best agreement with the experimental chemical shifts.^[18] The spectra simulation was carried out by using the gNMR 5.06 program.^[28] The synthesis and NMR spectra of derivatives **2–4** were described earlier.^[10] The procedures for the synthesis of **2a** and **3a** are given in the Supporting Information.

Supporting Information (see footnote on the first page of this article): Various ^1H NMR spectra of **2** and **4**, NOESY exchange spectra of a mixture of **2** and **2a** in CDCl_3 , table of experimental and calculated ^1H and ^{13}C NMR chemical shifts for derivatives **1–3** and **1a–3a**, fragments of ^{13}C NMR spectra of the trindone anion, and the procedure for the preparation of the bindone and trindone salts.

Acknowledgments

The financial support from the Israel Science Foundation (grant 135/06) is gratefully acknowledged.

- [1] W. Wislicenus, *Ber. Dtsch. Chem. Ges.* **1887**, *20*, 589–595.
- [2] D. Leblois, S. Piessard, G. Le Baut, P. Kumar, J. D. Brion, L. Sparfel, R. Y. Sanchez, M. Juge, J. Y. Petit, L. Welin, *Eur. J. Med. Chem.* **1987**, *22*, 229–238.
- [3] D. B. Hansen, M. M. Joulie, *Chem. Soc. Rev.* **2005**, *34*, 408.
- [4] K. Bello, L. Cheng, J. Griffiths, *J. Chem. Soc. Perkin Trans. 2* **1987**, 815.
- [5] M. R. Bryce, S. R. Davies, M. Hasan, G. J. Ashwell, M. Szablewski, M. G. Drew, R. Short, M. B. Hursthouse, *J. Chem. Soc. Perkin Trans. 2* **1989**, 1285–1292.
- [6] a) G. Meshulam, G. Berkovic, Z. Kotler, A. Ben-Asuly, R. Mazor, L. Shapiro, V. Khodorkovsky, *Ann. Isr. Phys. Soc.* **2000**, *14*, 71–74; b) G. Meshulam, P. Shaier, G. Berkovic, A. Ben-Asuly, R. Mazor, L. Shapiro, V. Khodorkovsky, Z. Kotler, *Non-linear Optics* **2000**, *25*, 321–326; c) H. Schwarz, R. Mazor, V. Khodorkovsky, L. Shapiro, J. T. Klug, E. Kovalev, G. Meshulam, G. Berkovic, Z. Kotler, S. Efrima, *J. Phys. Chem., B* **2001**, *105*, 5914–5921; d) A. Sombrata, P. Krief, V. Khodorkovsky,

- Z. Kotler, J. T. Klug, S. Efrima, *Acoust. Lett.* **2005**, 29, 1049–1057.
- [7] a) D. B. Ramachary, K. Anebuselvy, N. S. Chowdari, C. F. Barbas III, *J. Org. Chem.* **2004**, 69, 5838–5849; b) E. Stankovic, S. Toma, R. Van Boxel, I. Asselberghs, A. Persoons, *J. Organomet. Chem.* **2001**, 637–639, 426–434; c) I. Ledoux, J. Zyss, E. Barni, C. Barolo, N. Diulgheroff, P. Quagliotto, G. Viscardi, *Synth. Met.* **2000**, 115, 213–217.
- [8] M. W. Whitehouse, J. E. Leader, *Biochem. Pharmacol.* **1967**, 16, 537.
- [9] A. Hantsch, *Z. Phys. Chem.* **1913**, 84, 335.
- [10] K. Jacob, M. Sigalov, J. Y. Becker, A. Ellern, V. Khodorkovsky, *Eur. J. Org. Chem.* **2000**, 2047–2055.
- [11] a) N. Tyutyulkov, M. Tasseva, E. Georgiev, *J. Prakt. Chem.* **1987**, 329, 780–786; b) F. Dietz, N. Tyutyulkov, M. Rabinovitz, *J. Chem. Soc. Perkin Trans. 2* **1993**, 157–164.
- [12] a) G. Wanag, *Z. Anal. Chem.* **1938**, 113, 21–34; G. Wanag, *Z. Anal. Chem.* **1940**, 119, 413–417; b) V. Petrenko, *Zh. Anal. Khim.* **1980**, 35, 200–202 (CAN 92:220736).
- [13] G. Wanag, *Justus Liebigs Ann. Chem.* **1932**, 494, 107–116.
- [14] G. Wanag, *Ber. Dtsch. Chem. Ges.* **1935**, 68, 408–414.
- [15] M. Ionescu, H. Slusanschi, *Bull. Soc. Chim. Fr.* **1932**, 51, 1109–1125.
- [16] B. Zinger, P. Shaer, G. Berkovic, G. Meshulam, Z. Kotler, L. Shapiro, R. Mazor, V. Khodorkovsky, *Proc.-SPIE Int. Soc. Opt. Eng.* **1997**, 3135, 71–78.
- [17] M. L. de Winter, W. T. Nauta, *Eur. J. Med. Chem.* **1977**, 131–136.
- [18] M. Sigalov, A. Vashchenko, V. Khodorkovsky, *J. Org. Chem.* **2005**, 70, 92–100.
- [19] M. Sigalov, P. Krief, L. Shapiro, V. Khodorkovsky, *XVIII International Conference on Physical Organic Chemistry – Book of Abstracts*, **2006**, Warsaw, Poland, p.41.
- [20] G. R. Desiraju, *Acc. Chem. Res.* **1996**, 29, 441–449.
- [21] G. Bravic, G. Bravic, J. Gaultier, C. Hauw, *Cryst. Struct. Commun.* **1976**, 5, 5–8.
- [22] F. Hibbert, J. Emsley, *Adv. Phys. Org. Chem.* **1990**, 26, 255–379.
- [23] E. Kleinpeter, S. Klod, W.-D. Rudorf, *J. Org. Chem.* **2004**, 69, 4317.
- [24] M. J. Frisch, G. W. Trucks, H. B. Schlegel, G. E. Scuseria, M. A. Robb, J. R. Cheeseman, J. A. Montgomery Jr., T. Vreven, K. N. Kudin, J. C. Burant, J. M. Millam, S. S. Iyengar, J. Tomasi, V. Barone, B. Mennucci, M. Cossi, G. Scalmani, N. Rega, G. A. Petersson, H. Nakatsuji, M. Hada, M. Ehara, K. Toyota, R. Fukuda, J. Hasegawa, M. Ishida, T. Nakajima, Y. Honda, O. Kitao, H. Nakai, M. Klene, X. Li, J. E. Knox, H. P. Hratchian, J. B. Cross, C. Adamo, J. Jaramillo, R. Gomperts, R. E. Stratmann, O. Yazyev, A. J. Austin, R. Cammi, C. Pomelli, J. W. Ochterski, P. Y. Ayala, K. Morokuma, G. A. Voth, P. Salvador, J. J. Dannenberg, V. G. Zakrzewski, S. Dapprich, A. D. Daniels, M. C. Strain, O. Farkas, D. K. Malick, A. D. Rabuck, K. Raghavachari, J. B. Foresman, J. V. Ortiz, Q. Cui, A. G. Baboul, S. Clifford, J. Cioslowski, B. B. Stefanov, G. Liu, A. Liashenko, P. Piskorz, I. Komaromi, R. L. Martin, D. J. Fox, T. Keith, M. A. Al-Laham, C. Y. Peng, A. Nanayakkara, M. Challacombe, P. M. W. Gill, B. Johnson, W. Chen, M. W. Wong, C. Gonzalez, J. A. Pople, *Gaussian 03*, Revision B.05, Gaussian, Inc., Pittsburgh, PA, **2003**.
- [25] R. McWeeny, G. Dierksen, *J. Chem. Phys.* **1968**, 49, 4852; W. J. Hehre, R. Ditchfield, J. A. Pople, *J. Chem. Phys.* **1972**, 56, 2257.
- [26] R. G. Parr, W. Yang, *Density-Functional Theory of Atoms and Molecules*, Oxford University Press, Oxford, **1989**.
- [27] K. Wolinski, J. F. Hilton, P. Pulay, *J. Am. Chem. Soc.* **1990**, 112, 8251.
- [28] P. H. M. Budzelaar, *gNMR 5.0.6.0*, NMR Simulation Program, Copyright IvorySoft, **2006**.

Received: July 25, 2007

Published Online: November 28, 2007